Available online at www.sciencedirect.com
ScienceDirect
Journal of Sound and Vibration 299 (2007) 990–1004
JOURNAL OF SOUND AND VIBRATION
www.elsevier.com/locate/jsvi

In-duct orifice and its effect on sound absorption

R.C.K. Leung*, R.M.C. So, M.H. Wang, X.M. Li

Department of Mechanical Engineering, The Hong Kong Polytechnic University, Hung Hom, Kowloon, Hong Kong

Received 28 February 2006; received in revised form 12 June 2006; accepted 3 August 2006
Available online 28 September 2006

Abstract

A numerical investigation of sound absorption by an in-duct orifice with and without flow was carried out using a sixth-order finite difference direct numerical simulation (DNS) scheme with explicit fourth-order time marching to solve the governing Navier–Stokes equation. The DNS scheme has previously been validated against benchmark aeroacoustic problems and good agreement was obtained. Thus, it was applied to simulate the acoustic impedance of a circular orifice with different openings and a laminar flow through the same orifice. Both discrete frequency and broadband excitations were studied. When the in-duct orifice is exposed to discrete frequency sound wave in the absence of flow, alternate vortex shedding on both sides of the orifice is observed. The strength of shed vortices is stronger at low frequencies and thus the reduction of sound energy is higher. These vortices dissipate while moving away from the orifice. Therefore, the process provides a mechanism for adsorption of incident sound. The numerical results of broadband excitation indicate that small orifice opening is a more efficient sound absorber whereas a large opening is more or less transparent to the incident wave. The absorption, reflection and transmission coefficients of the in-duct orifice are calculated by a transfer function method. It is found that the sound coefficients are strongly dependent on the orifice opening size and frequency. In the presence of a flow, only alternate vortex shedding on one side of the orifice is observed. In spite of this, the results show that sound absorption behavior is very similar to the no flow case, i.e., sound absorption is more effective with small orifice.

1. Introduction

Flow ducts are commonly found in many aerospace and mechanical systems. The fluid inside the ducts is rarely able to flow through without encountering any obstructions or restrictions. Since such in-duct structural discontinuities are able to create drastic changes to the flow, they may be critical in determining the aero-acoustics and flow-induced vibration characteristics of the entire flow system. One of the most common types of in-duct structural discontinuity is an orifice, which is simply used to provide volume flow rate control. However, its presence may lead to a rather complicated interaction of sound waves with flows. In some situations, sound may be absorbed or generated as a result of this interaction.

The acoustical behavior of an orifice is highly nonlinear. Ingard and Ising [1] reported that the pressure fluctuations and oscillatory flow velocity could be approximately described by square-law relation at large

*Corresponding author. Tel.: +852 2766 6645; fax: +852 2365 4703.
E-mail address: mmrleung@inet.polyu.edu.hk (R.C.K. Leung).

0022-460X/$ - see front matter © 2006 Elsevier Ltd. All rights reserved.
doi:10.1016/j.jsv.2006.08.001

Nomenclature

c	speed of sound
D	size of the orifice opening
e	total energy per unit volume of the fluid
f	frequency of the incident sound
f_i	frequency of ith harmonic wave
H	duct width
M	Mach number
p	pressure of the fluid
$\hat{p}$	sound pressure of acoustic excitation
Pr	Prandtl number
p_0	static pressure at far upstream of the duct
P_{0i}	pressure amplitude of ith harmonic wave
Re	Reynolds number based on sound speed and duct width
Re_U	Reynolds number based on uniform flow speed and duct width
T	temperature at far upstream of the duct
t_f	period of the acoustic excitation
U	uniform flow speed
u, v	fluid velocity along x- and y-direction
φ_i	phase of ith harmonic wave
ρ	density of the fluid
ρ_0	density at far upstream of the duct
γ	ratio of specific heats
ν	kinematic viscosity
k'	thermal diffusivity
Δ_A, Δ_R, Δ_T	absorption, reflection and transmission coefficients

velocity amplitude. Cummings [2] proved using theoretical analysis and experiments that acoustic power-loss and flow-field induced by the orifice have strong nonlinearities. When a flow passes through an orifice in a duct, turbulence in the vicinity of the orifice may generate sound waves that propagate upstream and downstream of the orifice [3]. However, when the acoustic waves meet the orifice, the acoustic energy may be converted into kinetic energy of the flow near the orifice lips. A flow is generated due to an interaction of the sound field and the geometric discontinuity. Numerous studies on flow visualization and detailed velocity measurement [4,5] have been carried out to investigate the mechanism of sound absorption of an orifice at a duct end exposed to open air. The vortex shedding induced by the interaction of the orifice edge and acoustic wave is conjectured as being responsible for sound absorption. Jing and Sun [4] developed a quasi-steady potential model to study the acoustic impedance of an orifice varying from the incident sound intensity. Cummings [2] studied the net loss of the acoustic energy for the case that high-amplitude sound waves are released into open space through an orifice.

Cummings and Chang [6] and Wendoloski [7] studied the sound transmission and absorption for various Mach numbers for an orifice in a duct with a mean flow. According to the theoretical analysis of Wendoloski [7], it was found that the analysis was valid only when the duct mean flow Mach number is small compared with unity. Furthermore, for a mean flow Mach number less than 0.2, an orifice to duct opening ratio of 0.3 provides a near optimal average sound absorption. This was valid for the band of frequencies limited by the first symmetric mode cutoff frequency. Beyond these studies, to the best of the knowledge of the authors, there seem to be no more studies devoted to the investigation on the effect of mean flow on sound absorption by an orifice.

In spite of these exploratory studies, the mechanism of sound absorption by an in-duct orifice still remains rather unclear, even in the absence of a mean flow in a duct. Therefore, the objectives of the present study are two fold. The first is to explore the physical mechanism responsible for the absorption of sound by an in-duct orifice and find the relations between sound absorption, frequencies and opening sizes using a one-step method to calculate the aeroacoustics field. The vehicle of this calculation is the direct numerical simulation (DNS) of the governing unsteady compressible Navier–Stokes equation. This part of the investigation is carried out in the absence of a mean flow in the duct. Detailed behavior of the acoustic waves impinging on the orifice and their transmission through it is investigated. The effect of orifice size on this behavior is studied. The second objective is to investigate the effect of a mean flow on this behavior for the range of orifice sizes examined. Only one Reynolds number is considered. Finally, the sound absorption coefficient of the orifice is deduced for the two cases with and without flow; thus allowing an estimate on sound absorption to be made and the effect of orifice size on sound absorption.

2. Problem formulation and numerical method

Two-dimensional (2-D) incident sound waves propagating towards an orifice with opening size D installed at the origin inside a duct with width H are considered. The definition of the computational domain is illustrated in Fig. 1. The upstream portion of the duct has a length $L_{\text{up}} = 3H$ and the downstream portion has a length $L_{\text{down}} = 8H$. The governing equations are the 2-D unsteady compressible Navier–Stokes equation. Written in strong conservation form, the equation can be expressed in Cartesian coordinates (x, y) as

$$\frac{\partial \mathbf{Q}}{\partial t} + \frac{\partial \mathbf{E}}{\partial x} + \frac{\partial \mathbf{F}}{\partial y} = \frac{\partial \mathbf{E}_v}{\partial x} + \frac{\partial \mathbf{F}_v}{\partial y}, \tag{1}$$

where the vectors $\mathbf{Q}$, $\mathbf{E}$, $\mathbf{F}$, $\mathbf{E}_v$ and $\mathbf{F}_v$ are given by

$$\mathbf{Q} = [\rho, \rho u, \rho v, \rho e]^{\mathrm{T}}, \tag{2a}$$

$$\mathbf{E} = \left[\rho u, \rho u^2 + p, \rho uv, u(\rho e + p)\right]^{\mathrm{T}}, \tag{2b}$$

$$\mathbf{F} = \left[\rho v, \rho uv, \rho v^2 + p, v(\rho e + p)\right]^{\mathrm{T}}, \tag{2c}$$

$$\mathbf{E}_v = \left[0, \tau_{xx}, \tau_{xy}, u\tau_{xx} + v\tau_{xy} + q_x\right]^{\mathrm{T}}, \tag{2d}$$

$$\mathbf{F}_v = \left[0, \tau_{xy}, \tau_{yy}, u\tau_{xy} + v\tau_{yy} + q_y\right]^{\mathrm{T}}. \tag{2e}$$

The total energy per unit volume is defined as $e = p/(\gamma - 1) + \rho\left(u^2 + v^2\right)/2$, where $\gamma = c_p/c_v = 1.4$, is the ratio of the specific heats. The stress tensor components are given by

$$\tau_{xx} = \frac{2}{3}\mu\left(2\frac{\partial u}{\partial x} - \frac{\partial v}{\partial y}\right), \tag{3a}$$

$$\tau_{xy} = \frac{2}{3}\mu\left(\frac{\partial u}{\partial y} - \frac{\partial v}{\partial x}\right), \tag{3b}$$

$$\tau_{yy} = \frac{2}{3}\mu\left(2\frac{\partial v}{\partial y} - \frac{\partial u}{\partial x}\right), \tag{3c}$$

where μ is fluid viscosity, and (q_x, q_y) are heat flux along the (x, y) direction. These equations can be made dimensionless by normalizing the variables using the height of the square duct H, the speed of sound c, the density ρ_0 and temperature T_0 far upstream of the duct.

A DNS method is used to treat the nondimensional governing equations which are solved by a sixth-order compact finite-difference scheme and an explicit fourth-order Runge–Kutta time marching technique [8]. The tenth-order filtering derived by Visbal and Gaitonde [11] is applied in every final stage of the Runge–Kutta scheme to suppress numerical instabilities due to spatial differencing. The mesh is designed to have enough resolution to make sure that the Stokes layer and high-frequency acoustic waves can be resolved correctly. The minimum mesh size $\Delta x/H$ is 2×10^{-3}. No-slip conditions are applied to the orifice surface and all duct walls. A perfectly matched-layer (PML) non-reflecting condition with the same damping function prescribed in Ref. [9] is applied at the duct inlet and outlet with buffer region width given by $D_I/H = 1$ and $D_O/H = 2$,

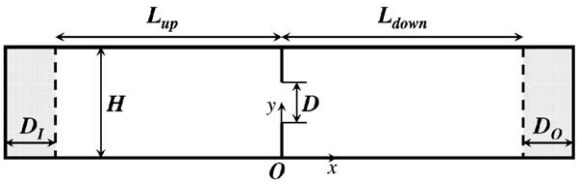

Fig. 1. Schematic of computational domain.

respectively (Fig. 1). The Reynolds number is defined as $Re = cH/v = 10000$, where v is the fluid kinematic viscosity. This Re is required to be specified because it appears in the final set of nondimensional equations. The incident sound pressure amplitude is fixed at 0.1% of the static pressure far upstream which corresponds to an incident sound pressure level of approximately 131 dB.

The incident sound is assumed to originate from a continuously repeated pulse generated far upstream and composed of a series of harmonic waves defined as follows:

$$P = \sum_{i=1}^{n} P_{0i} \cos(2\pi f_i t + \varphi_i), \tag{4}$$

where P_{0i}, f_i and φ_i are, respectively, the amplitude, frequency and phase of the ith harmonic wave. The values of phase φ_i are generated from random number generator. Therefore, the harmonic waves expressed in Eq. (2) are not correlated and they altogether represent an essentially broadband incident sound. Calculations with discrete incident frequencies were carried out to study the sound-induced flow and the associated sound absorption. Excitation with broadband incident sound is used to determine the variations of reflection, absorption and transmission coefficients with orifice parameters. The frequency range of the incident sound waves is $0.07 \leqslant fH/c \leqslant 1.02$, where c is the ambient speed of sound. The dimensionless orifice size D/H is chosen to take the values of 0.05, 0.2, 0.4, 0.6 and 0.8. The Mach number is defined as $M = U/c$, where U is the mean flow velocity in the far upstream of the duct. This numerical scheme has been briefly discussed in Ref. [8] and is available elsewhere [10,11]; therefore, they will not be repeated here. Interested readers could refer to Refs. [10,11] for details.

3. Evaluation of sound coefficients

When a sound wave is incident on an in-duct orifice, it may be reflected, transmitted or absorbed by the orifice. The levels of reflection, transmission or absorption vary with the frequency of the sound wave. These acoustic phenomena are best determined by comparing their respective intensity with respect to the incident sound intensity and expressed in terms of sound coefficients. The following describes a method to determine the in-duct sound coefficients based on the transfer function method described by Chung and Blaser [12,13].

Assume a 2-D linear plane wave propagates from far upstream and interacts with the orifice. The sound pressure at any frequency may be decomposed into two parts in different directions,

$$\hat{p} = \hat{p}^{+} \mathrm{e}^{-\mathrm{j}\hat{k}^{+}x} + \hat{p}^{-} \mathrm{e}^{-\mathrm{j}\hat{k}^{-}x}, \tag{5}$$

where $\hat{p}^{+}$ and $\hat{p}^{-}$ are the complex spectral amplitudes of forward and backward propagating wave components, $\hat{k}^{+}$ and $\hat{k}^{-}$ are forward and backward complex wave numbers, respectively. The caret symbol on top of the variables expresses the complex variable

$$\hat{k}^{+} = \frac{k + \alpha(1-j)}{(1+M)} \quad \text{and} \quad \hat{k}^{-} = \frac{k + \alpha(1-j)}{(1-M)}, \tag{6a,b}$$

$$\alpha = (1/Hc)\left(v2\pi f/2\right)^{1/2}\left[1 + (\gamma - 1)Pr^{-1/2}\right], \tag{7}$$

where $k = 2\pi f/c$, $Pr = v/k'$ is the Prandtl number and k' is the thermal diffusivity. The time histories of the pressure fluctuations at two chosen locations, namely $p_1(t)$ and $p_2(t)$ are recorded during the calculation. The values of $\hat{p}^{+}$ and $\hat{p}^{-}$ can then be calculated from the expressions

$$\left|\hat{p}^{+}\right| = \frac{G_{11}^{1/2}}{\left|1 + \hat{R}\right|} \quad \text{and} \quad \hat{p}^{+} = \hat{R}\hat{p}^{-}, \tag{8a,b}$$

$$\hat{R} = -\left\{\frac{\hat{G}_{12} - G_{11}\,\mathrm{e}^{-\mathrm{j}\hat{k}^{+}l}}{\hat{G}_{12} - G_{11}\,\mathrm{e}^{-\mathrm{j}\hat{k}^{-}l}}\right\}, \tag{8c}$$

where G_{11}, G_{22} and $\hat{G}_{12}$ are, respectively, the auto-spectra and cross-spectrum of p_1 and p_2. The sound intensity of the forward and backward propagating wave components can be calculated using the equations [14,15]

$$I^+ = \frac{1}{\rho_0 c_0}\left|\hat{p}^+\right|^2(1+M)^2, \tag{9a}$$

$$I^- = \frac{1}{\rho_0 c_0}\left|\hat{p}^-\right|^2(1-M)^2. \tag{9b}$$

In the present investigation, the acoustic coefficients of the orifice were evaluated from I^+ and I^- calculated at the locations on both sides of the orifice as illustrated in Fig. 2. The reflection (Δ_R) and transmission (Δ_T) coefficients are defined as the proportion of incident acoustic power flux reflected from and transmitted through the orifice. As the cross-sectional area of the upstream and downstream portions of the duct is the same, the coefficients can be expressed as

$$\Delta_R = \frac{\left|I^-_{\mathrm{up}}\right|}{\left|I^+_{\mathrm{up}}\right|} \quad \text{and} \quad \Delta_T = \frac{\left|I^+_{\mathrm{down}}\right|}{\left|I^+_{\mathrm{up}}\right|}. \tag{10a,b}$$

The definition of absorption (Δ_A) coefficient needs more thorough consideration. In the theoretical analysis of the absorption of an in-duct element, for example an abrupt area expansion [16], the duct portions upstream and downstream of the element are usually assumed infinitely long. Essentially the incident sound wave is assumed to propagate from $x=-\infty$ and hit the in-duct orifice at $x=0$ (Fig. 2). This incident sound is partly reflected and partly transmitted into the downstream portion of the duct. The transmitted sound wave will then propagate towards $x=+\infty$ and never comes back to the orifice. However, all practical ducts in engineering situations are of finite length [15,16]. The transmitted sound wave might be reflected at the duct outlet. If $k/H<\pi$ and kL_{down} is large, this reflected sound wave will be planar and is equivalent to a second sound wave propagating from $x=-\infty$ towards the orifice. In most numerical and experimental studies, the duct is of finite length, this second incident sound exists due to the finite acoustic impedance at the outlet. For instance, in the calculations with $D/H=0.4$ and a broadband incident wave, the average $\left|I^-_{\mathrm{down}}\right|$ was found to be approximately equal to 4.5% of the average of $\left|I^+_{\mathrm{up}}\right|$. This small but finite amount of $\left|I^-_{\mathrm{down}}\right|$ reveals that the PML used in the present study might not be able to truly replicate the sound propagation towards $x=-\infty$. Therefore, the definition of the absorption should take the second incident sound wave into account and should be defined as

$$\Delta_A = \frac{\left|I^+_{\mathrm{up}} + I^-_{\mathrm{down}} - I^-_{\mathrm{up}} - I^+_{\mathrm{down}}\right|}{\left|I^+_{\mathrm{up}}\right| + \left|I^-_{\mathrm{down}}\right|}. \tag{10c}$$

It should be pointed out that the accuracy of Eqs. (10a)–(10c) depends on the separation l between two measurement locations. This l should be kept to within one-half wavelength of the highest frequency of interest, i.e. $lf/c<0.5$. On the other hand, the measurement locations should be far away from the orifice to avoid any nonlinearity that violates the linear assumption of Eqs. (5)–(9).

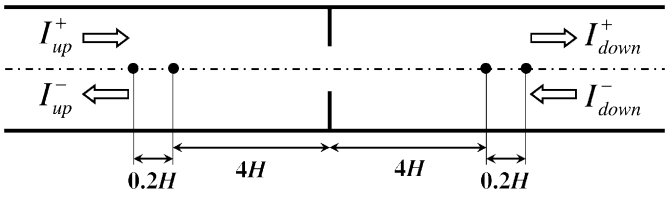

Fig. 2. Measurement locations for the calculation of sound coefficients.

4. Validation

Before analyzing the sound absorption of an in-duct orifice, the numerical model has to be validated. Since the present problem involves nonlinear interaction between sound waves and unsteady vortex shedding at an orifice lip, the numerical model has to be capable of resolving the unsteady flow and linear acoustics correctly. In the present investigation, the capability of unsteady flow calculation is assessed by comparing the DNS calculated results with experiments of a laminar flow over a backward facing step and through an in-duct orifice. The experimental study of a back-step flow [17] and nonlinear acoustic response of an orifice [5] is used to assess the correctness of acoustics calculation.

The present study focuses on the acoustics field and this requires careful treatment of the boundaries, especially if they were to be truly non-reflecting so that there will be no spurious waves bouncing back to contaminate the aeroacoustic simulation. In view of the great disparity in scales between the aerodynamic and acoustic field (10^{-3}–10^{-5}), even a small error in the aerodynamic solution could create spurious acoustics waves that could greatly affect the simulation result. Therefore, it is necessary to ascertain that the basic aerodynamic solution is correct before confidence could be established for the acoustic simulation. The first step of this validation is to carry out an aerodynamic simulation of an experimental back-step flow and compared the calculated results with measurements. A comparison of this 2-D flow has previously been carried out by the authors [8] and good agreement was obtained for the measured and calculated reattachment and separation lengths. The non-reflecting boundary conditions were then tested by comparing the acoustic power W of continuous acoustic pulses propagating through the duct with a backward facing step. Theoretically, the back-step flow is like a low-pass filter to the acoustic waves. Low frequency waves could pass and propagate for a long distance downstream. High frequency waves are strongly attenuated. Their comparisons clearly showed that PML is best for all three frequencies tested, low to high. Since these results [8] have been reported before, it will not be repeated here.

Direct measurement of acoustic nonlinearity of an in-duct orifice is rare in the literature. Jing and Sun [5] developed a theoretical model for the acoustic impedance of an in-duct orifice and compared with experiments. Using impedance tube method with two-microphone technique, they measured the acoustic impedance of a circular orifice with 4 mm radius that was placed in a square duct of 100×100 mm cross section. This setup gave $D/H = 0.08$ with regard to the hydraulic diameters of the orifice and the duct cross sections. Discrete-frequency sound waves were generated by four loudspeakers placed at the duct inlet and the sound pressure level just upstream of the orifice was measured at approximately 144 dB. An anechoic termination was placed at the duct outlet to suppress any reflection back to the orifice. The acoustic impedance is in general complex. Its real and imaginary parts, z_r and z_x, represent the resistance and reactance of the sound propagation, respectively. It was observed that the values of z_r and z_x depend on both the amplitude and frequency of the incident sound waves. For simplicity, the comparison with experiment was made with calculations with constant pressure-amplitude excitation using the same D/H and sound pressure level. The calculated specific acoustic impedance as a function of normalized sound pressure is plotted in Fig. 3. The impedance and the sound pressure are normalized by $\rho_0 fH$. The normalized quantities are $Z_r = z_r/\rho_0 fH$, $Z_x = z_x/\rho_0 fH$. It should be noted that the normalized sound pressure is effectively treated as a parameter for frequency variation. The calculated frequency variations of Z_r and Z_x thus plotted match closely with experimental results. This suggests that the present numerical model is capable of calculating the acoustics inside a duct correctly.

5. Results and discussions

A series of numerical simulations were carried out for the acoustic field and the flow field driven by incident acoustic waves across an orifice in a duct with and without a mean flow. In order to make direct comparison of the sound absorption between the cases with and without the mean flow in the duct, both numerical simulations of the case with and without a mean flow were performed separately. The simulation for each case was carried out in a one-step manner, i.e., the governing unsteady Navier–Stokes equations were solved for both the aerodynamic and acoustics field simultaneously. It was not necessary to solve the wave equation separately after the aerodynamic solution was obtained. For the case without flow, a continuous train of

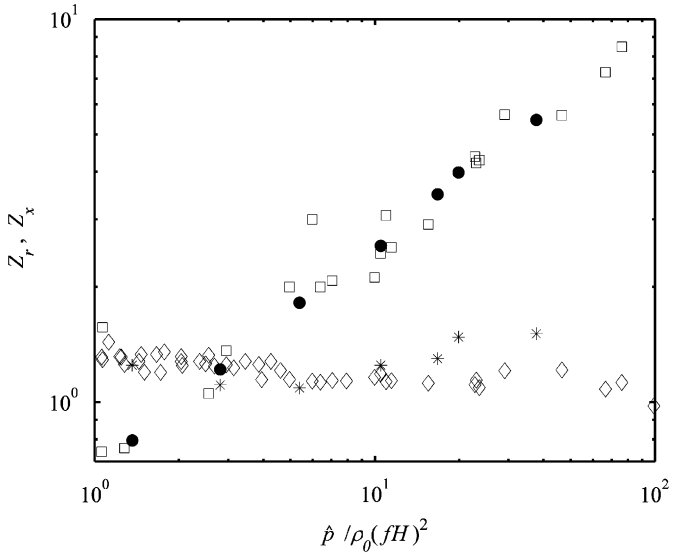

Fig. 3. Acoustic nonlinearity of in-duct orifice with $D/H = 0.08$. Experiments of Jing and Sun [5]: (□) acoustic resistance Z_r; and (◇) acoustic reactance; Z_x. Present calculations: (●) acoustic resistance Z_r; and (∗) acoustic reactance Z_x.

sound pulses with either single or broadband frequencies was input to the duct in the upstream end. When the sound with a single frequency was input to the duct, the flow field and vortex shedding thus excited were studied in detail. Only the case with broadband sound input was used to examine the sound absorption behavior and its dependence on frequencies. The sound absorption, transmission and reflection coefficients were deduced from Eqs. (10a)–(10c) after the acoustic field was determined. Since the present focus is on sound absorption by the orifice, in the following, only Δ_A is compared for the case with and without flow. Only one case with flow was studied and this was carried out with orifice opening to duct width ratio $D/H = 0.05$, 0.2, 0.4, 0.6 and 0.8. The input sound is broadband and the Reynolds number and Mach number for this case is $Re_U = 100$ and $M = 0.01$. At this Re_U, the flow is laminar. The discussion is organized into three subsections; each is devoted to a thorough discussion of the following phenomena.

5.1. Sound-excited vortex shedding

When a sound wave is passing through the orifice, the periodic sound pressure fluctuation induces local periodic velocity fluctuation, resulting in flow separation under the action of viscosity and subsequent shedding of vortices at the orifice lip. Fig. 4 illustrates the vortex shedding from a narrow orifice ($D/H = 0.05$) with sound excitation at $fH/c = 0.1$. Only the variations within one excitation period are shown. The starting time t_0 corresponds to the moment when sound pressure at the orifice center achieves its maximum. The period of sound wave is indicated by t_f. At t_0 the pressure gradient creates a local flow in the upstream direction and generates a puff of vorticity on the upstream side of the orifice lip. The vorticity puff takes its maximum strength after one-quarter cycle ($t_0 + t_f/4$) of pressure fluctuation and then completely shed as a vortex (A) upstream at $t_0 + t_f/2$. At this moment the direction of the local flow through the orifice reverses and a new puff of vorticity is created on the downstream side of the orifice. This new vorticity puff attains its maximum strength at $t_0 + 3t_f/4$ and is completely shed as a new vortex (B) at $t_0 + t_f$. The shed vortices can only last for three periods and will eventually fully dissipate due to the action of viscosity. The distributions of sound pressure fluctuations in the duct at different t are also illustrated in Fig. 4. It can be seen that the effect of vortex shedding on sound propagation is confined to the vicinity of the orifice opening. Farther downstream the sound propagated merely as plane waves. The spectra of vorticity and pressure fluctuation are plotted in Fig. 5, which clearly shows the coincidence of the vortex shedding frequency and the incident sound frequency. It indicates that vortex shedding is solely driven by the sound wave. Evidently the sound-excited vortex

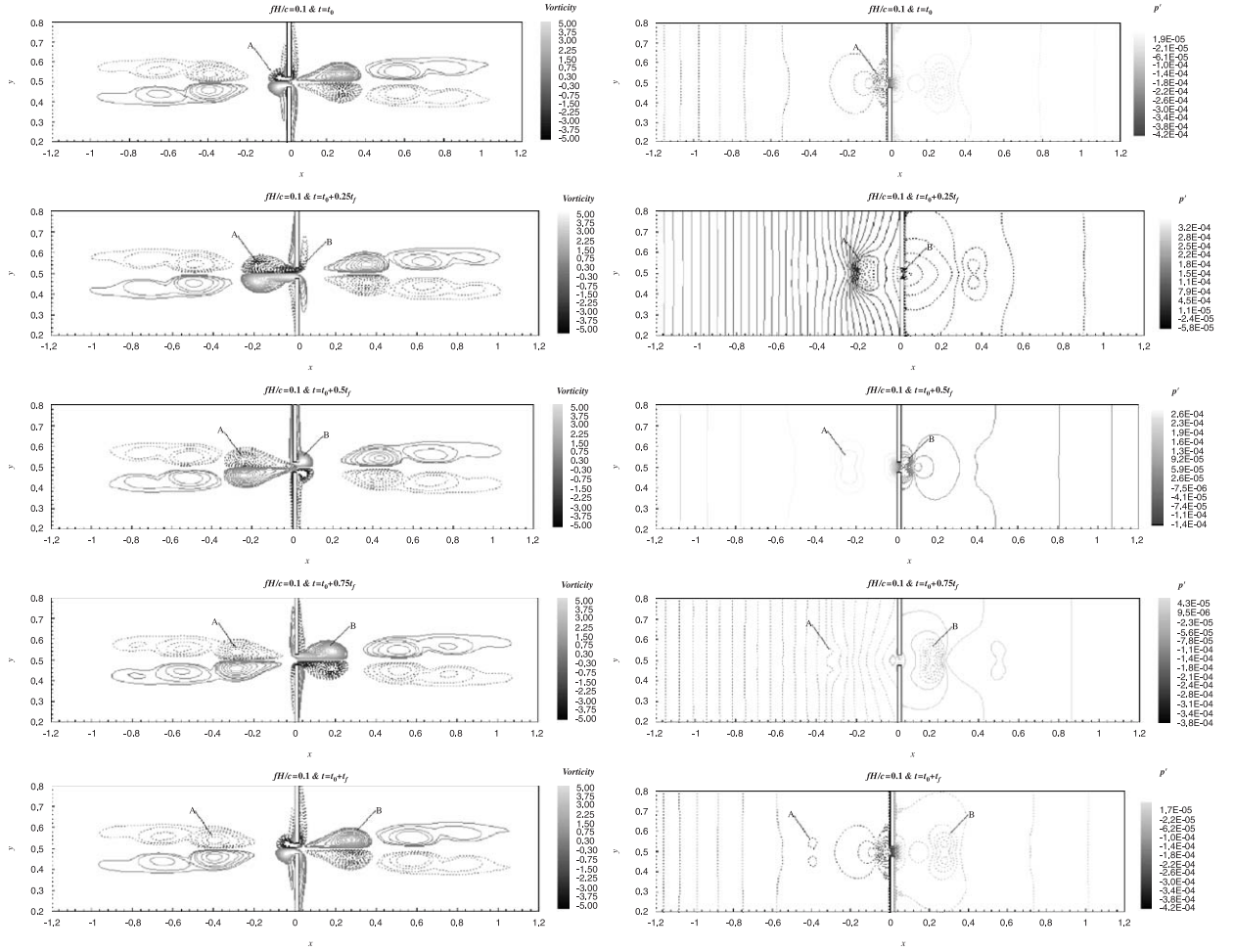

Fig. 4. Plots of vortex shedding and pressure fluctuations within one period of a sound wave for $D/H = 0.05$. The moving vortex pairs A and B are labeled in the figures. Left column indicates vortex shedding while the right column indicates pressure fluctuations.

shedding from the orifice lip together with subsequent viscous dissipation provides an effective process for the dissipation of sound.

The frequency of incident sound wave is critical to the sound-excited vortex shedding. Fig. 6 illustrates the vorticity distributions around the same orifice excited by sound with $fH/c = 0.2$, 0.5 and 1.0. It can be observed that the higher the excitation frequency becomes, the weaker is the vorticity produced. When $fH/c = 0.2$, pairs of vorticity puffs emerge from the orifice lip and dissipate. No clear vortex shedding can be observed. At higher frequency, only a thin boundary layer can be observed in the orifice. The strength of the boundary layer vorticity generally decreases with increasing frequency. The observed frequency dependence implies that the sound dissipation by vortex shedding from the orifice is only possible with low frequency sound. With a high frequency pressure fluctuation, the sound-induced local velocity fluctuation changes so rapidly that it inhibits any vortex shedding.

The orifice size opening also has a great effect on vortex shedding. Fig. 7 illustrates the variations of vorticity and sound pressure fluctuations of an orifice with $D/H = 0.4$ during one period of excitation. The excitation frequency $fH/c = 0.1$. It is evident that a large orifice size tends to create weak vortices as a result of weaker local velocity fluctuations induced at the orifice opening. These vortices dissipate quickly after shedding. Consequently, the incident sound propagates along the duct with minor distortion while it is passing through the orifice.

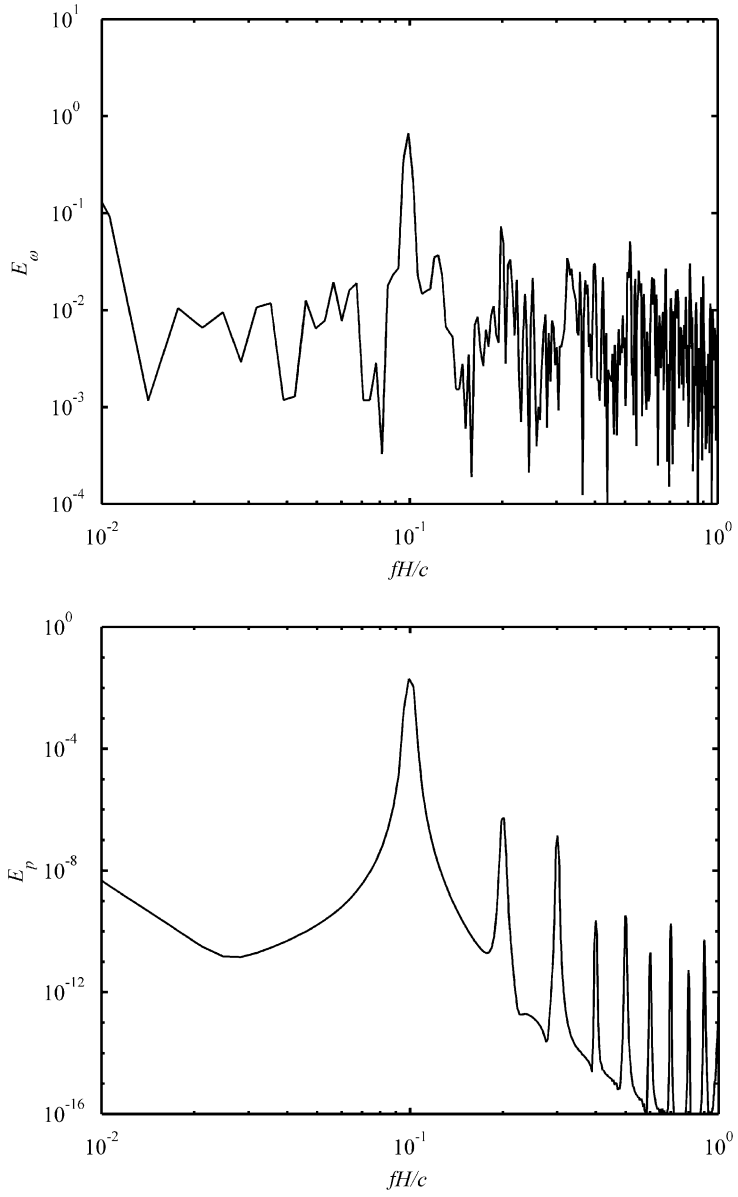

Fig. 5. Spectra of vorticity E_ω and pressure fluctuations E_p at $(x/H, y/H) = (0.5, 0.55)$ with $D/H = 0.05$ and $fH/c = 0.1$.

5.2. Sound absorption coefficient (Δ_A)

The forgoing section describes the mechanism of sound absorption of orifice due to vortex shedding and its effectiveness with discrete frequency excitation. For a complete description of nonlinear acoustic behavior, the coefficients of sound reflection, transmission and absorption are calculated by exciting the orifice with a broadband incident sound of the same pressure amplitude, as described in Section 3. The calculated coefficients for $D/H = 0.05$, 0.2, 0.4, 0.6 and 0.8 are illustrated in Fig. 8. It can be observed that Δ_A is strongly dependent on the orifice opening and frequency. The larger is the orifice opening, the weaker is the sound absorption. Furthermore, the absorption is sensitive to the incident frequency and the occurrence of absorption peaks changes with the opening size. For $D/H = 0.05$, high absorption of acoustic energy is found

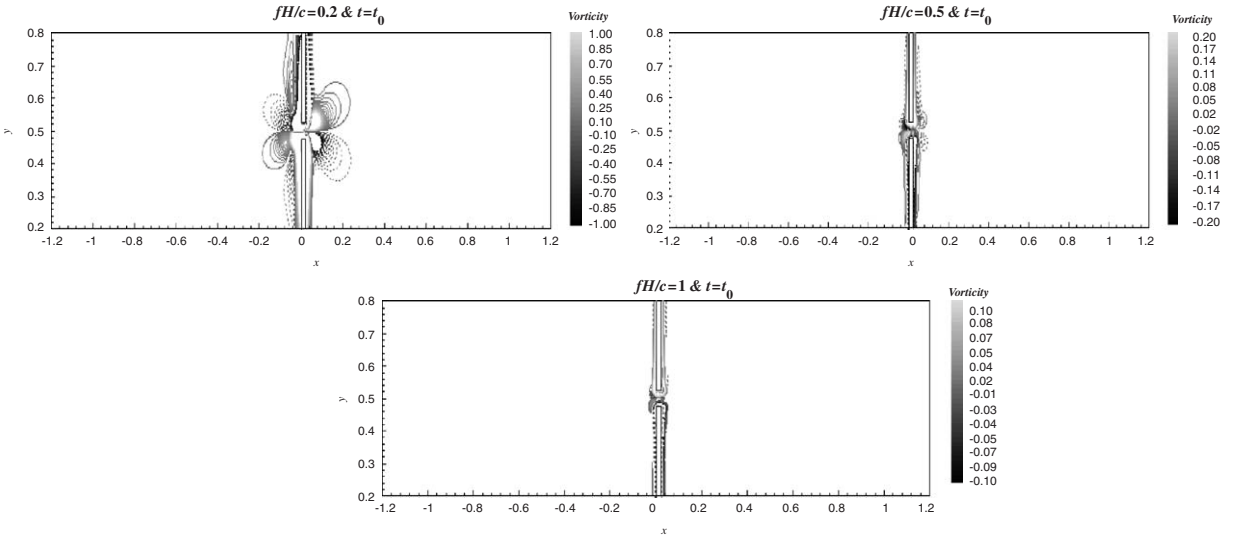

Fig. 6. Vortex shedding from an orifice with $D/H = 0.05$ at various incident frequencies.

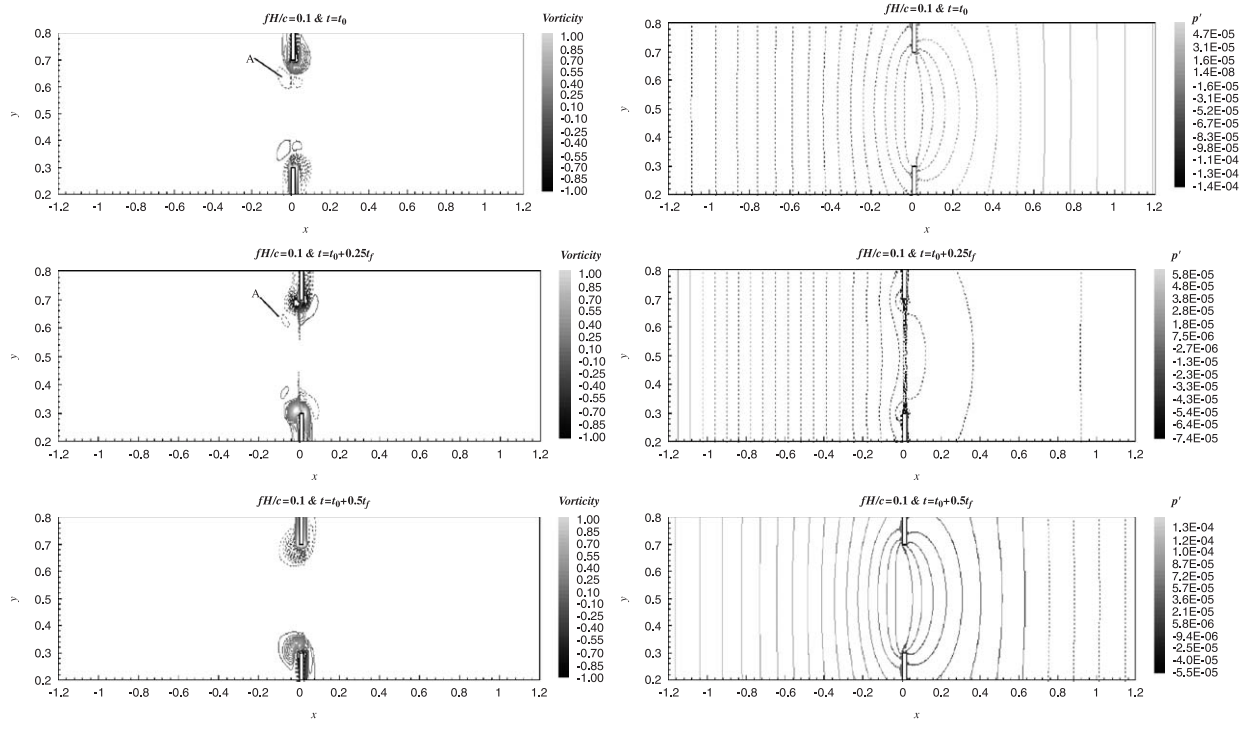

Fig. 7. Plots of vortex shedding and pressure fluctuations within one period of a sound wave for $D/H = 0.4$. Left column indicates vortex shedding while the right column indicates pressure fluctuations.

at the frequency $fH/c = 0.14$ and 0.52, minimum absorption at $fH/c = 0.32$ and 0.75. Reflection and transmission coefficients (Δ_R and Δ_T) also vary with opening size and frequency. When Δ_R reaches maximum values, Δ_A and Δ_T are at their minimum values. The above observation clearly indicates that sound absorption of the orifice is strongly dependent on the acoustical compactness, i.e., the ratio of the orifice opening to the incident wavelength of the sound-induced flow.

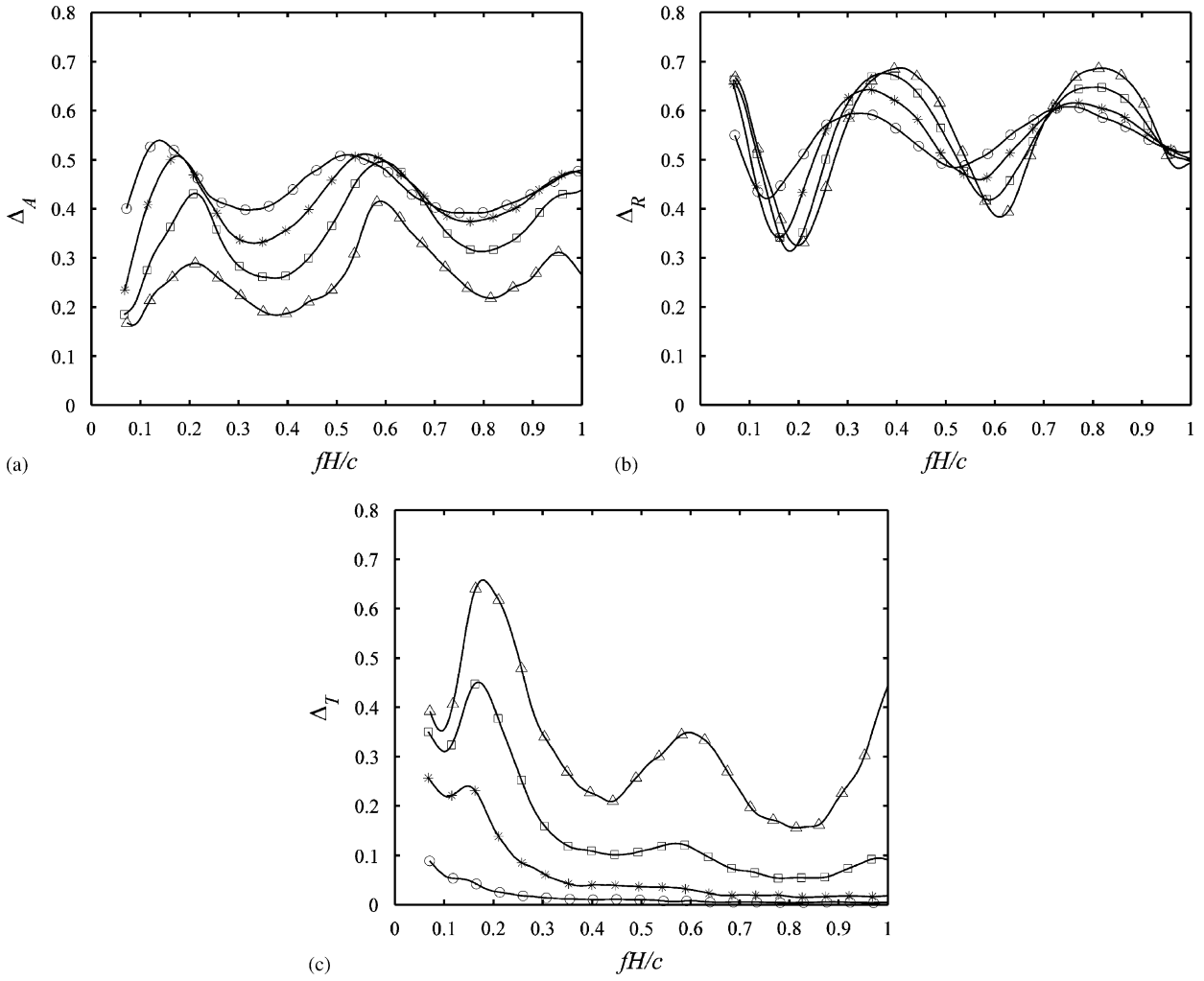

Fig. 8. Variations of acoustic coefficients with frequencies: (a) absorption coefficient; (b) reflection coefficient; and (c) transmission coefficient. (—○—) $D/H = 0.05$; (—*—) $D/H = 0.2$; (—□—) $D/H = 0.4$; and (—△—) $D/H = 0.6$.

5.3. Effect of mean flow

Having examined the case where there is no mean flow, the next task is to study the case where $Re_U = 100$ and $M = 0.01$. In this set of calculations, only the case where broadband sound is input to the duct inlet is investigated in detail for $D/H = 0.05$, 0.2, 0.4, 0.6 and 0.8. Sample plots of vorticity and pressure fluctuations similar to those shown in Fig. 4 are plotted in Fig. 9. Only two D/H cases are shown; one with very small opening ($D/H = 0.05$) and another with fairly large opening ($D/H = 0.6$). The vorticity and pressure fluctuations are calculated using the total vorticity and pressure minus the mean vorticity and pressure. It can be seen from Fig. 9 that in the presence of a mean flow in the duct, the shed vortices from the orifice tips orient themselves into one direction only and that is the flow direction. Vortex shedding in the opposite direction is restricted. The vortex indicated as A in Fig. 4 (see the panel given by $t = t_o$) is absent from Fig. 9. Therefore, only one row of the vortex pairs occurs in the flow field. The mean flow facilitates the renascent vortices to shed from the orifice tips and transport them quickly away along the mean flow direction. There are obvious differences in the distribution of the pressure fluctuations too. In the first place, the pressure fluctuations downstream of the orifice are much stronger. In the second place, the pressure fluctuations around the orifice (upstream and downstream of the orifice) are quite different from those shown in Fig. 4; a more uniform

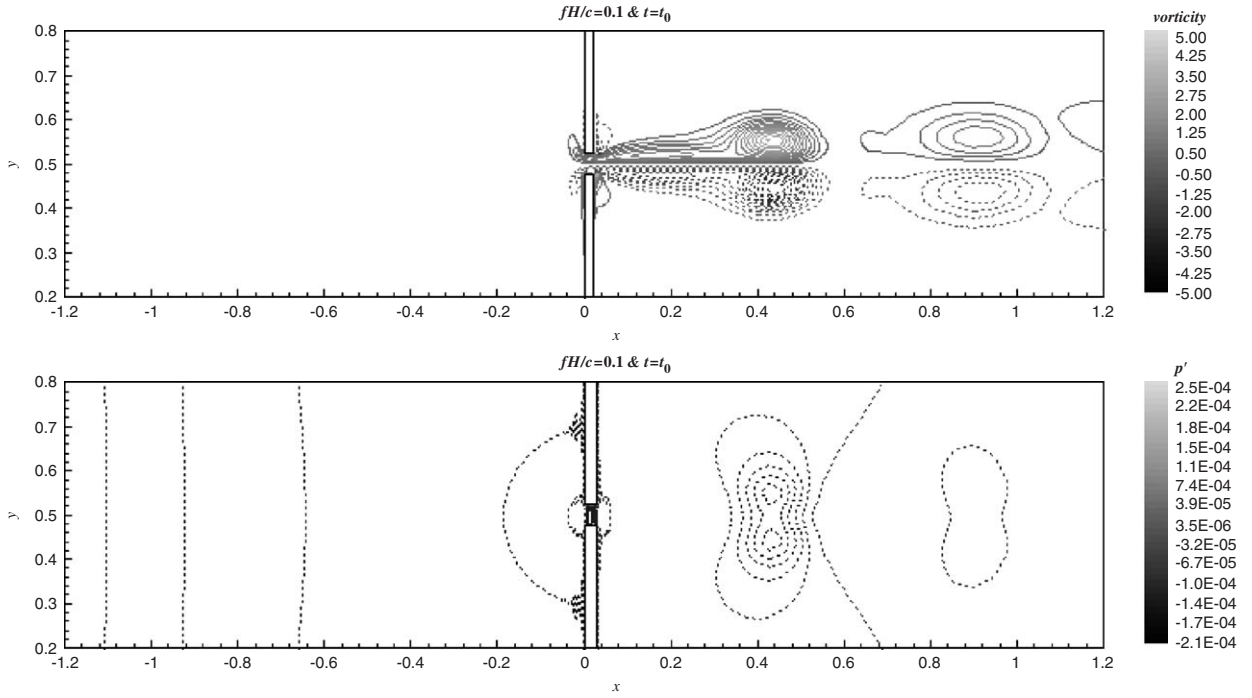

Fig. 9. Vorticity and pressure contours in the duct for the case where $Re_U = 100$ and $D/H = 0.05$.

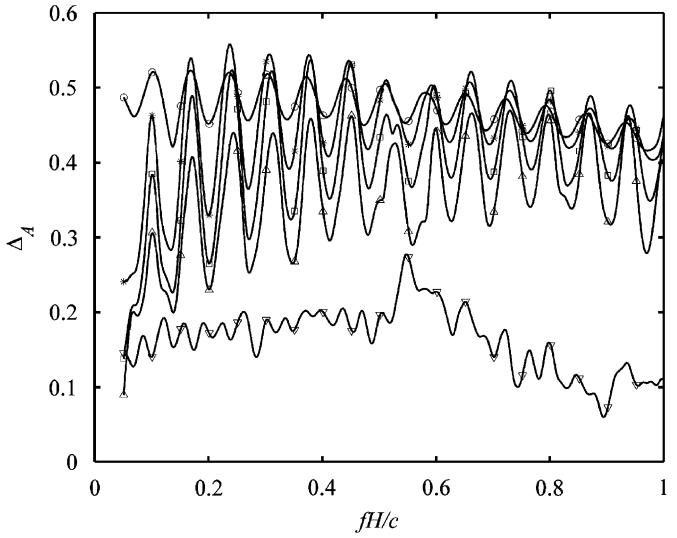

Fig. 10. Variations of absorption coefficient with frequencies in the presence of a mean flow ($Re_U = 100$, $M = U/c = 0.01$). (—○—) $D/H = 0.05$; (—*—) $D/H = 0.2$; (—□—) $D/H = 0.4$; (—△—) $D/H = 0.6$; and (—▽—) $D/H = 0.8$.

distribution is achieved sooner for the $Re_U = 0$ case than for the $Re_U = 100$ case. Consequently, the mean flow changes the vortex shedding and pressure distribution behavior, hence the sound absorption mechanism.

The calculated Δ_A are plotted in Fig. 10 for $D/H = 0.05$, 0.2, 0.4, 0.6, and 0.8. Its behavior as a function of the normalized frequency is very similar to those shown for the case $Re_U = 0$ (Fig. 8). There are some differences in the detailed behavior of Δ_A as a function of fH/c though. However, the overall level of Δ_A for a given D/H is essentially the same as the $Re_U = 0$ case (Fig. 8). A direct comparison of Δ_A for these two cases is

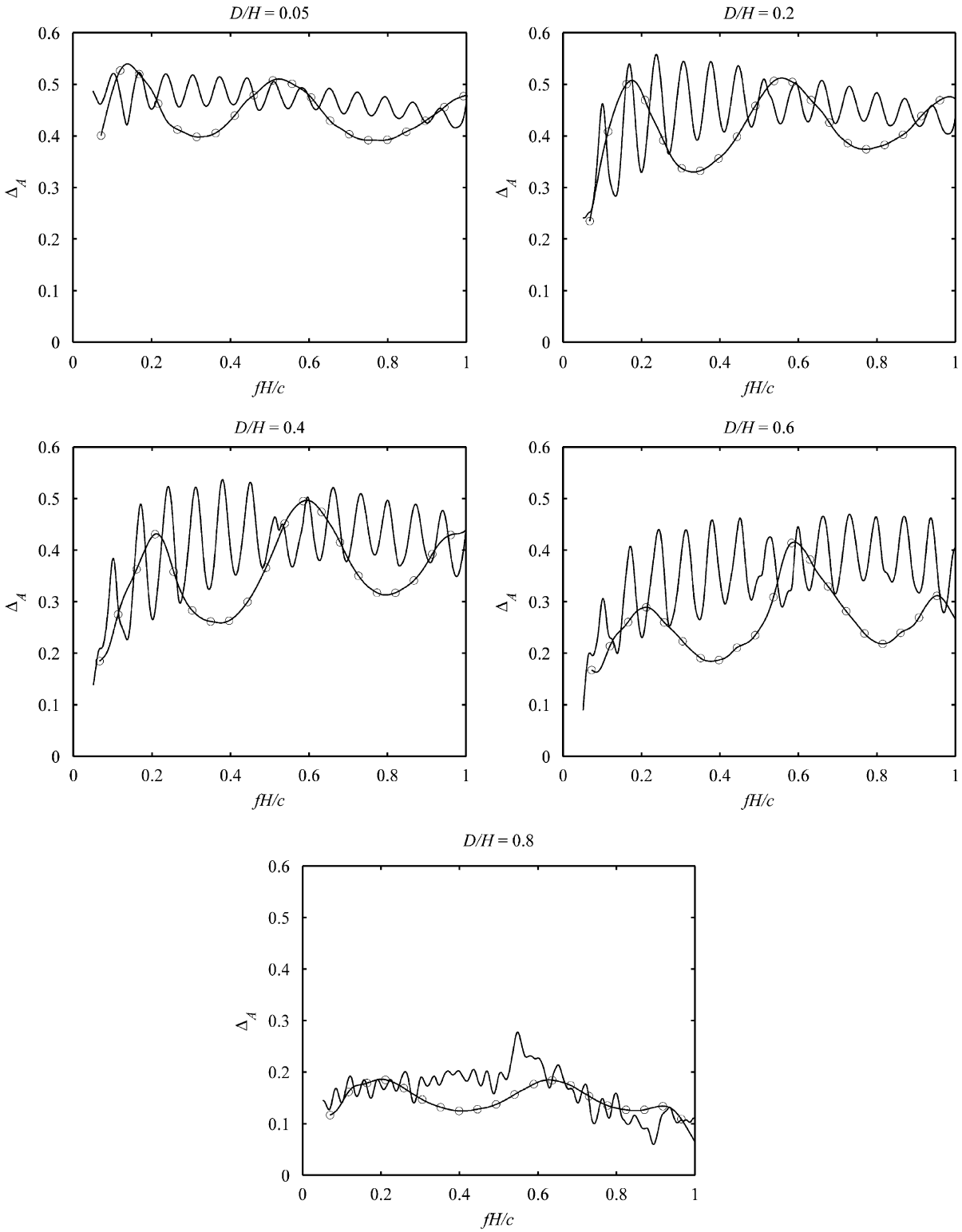

Fig. 11. Comparison of the absorption coefficient of an in-duct orifice with and without mean flow. (———) $Re_U = 0$; (—○—) $Re_U = 100$ ($M = U/c = 0.01$).

shown in Fig. 11 where the Δ_A vs. fH/c curves are plotted separately for each D/H. Altogether there are five panels in Fig. 11, one for each D/H. This comparison clearly shows that there is no significant advantage in Δ_A for the $Re_U = 100$ case over that of the $Re_U = 0$ case other than for fH/c around 0.3–0.4 and around 0.8 there is a dip in Δ_A for the $Re_U = 100$ case. As expected, the lowest Δ_A is found in the case where $D/H = 0.8$ while the highest is given by the case where $D/H = 0.05$. This finding that a mean flow has essentially no effect on Δ_A appears to be different from that deduced by Wendoloski [7].

6. Conclusions

A numerical study of sound absorption by an in-duct orifice is reported. The problem is simulated by a one-step aeroacoustics method using a sixth-order finite difference DNS with explicit fourth-order time marching. The numerical scheme was validated by comparing the numerical calculations with two experiments, namely laminar flow through an in-duct orifice and the acoustic impedance of a circular orifice. The good agreement with experimental results establishes the accuracy of the numerical calculations and validates the scheme. When the in-duct orifice is exposed to discrete frequency sound wave, alternate vortex shedding on both sides of the orifice is observed. The shed vortices convect only a short distance and dissipate. The strength of shed vortices is stronger at low frequencies and thus the reduction of sound energy is higher. These processes provide a mechanism for adsorption of incident sound. The numerical results of broadband excitation indicate that small orifice opening is a more efficient sound absorber whereas a large opening is more or less transparent to the incident wave. The absorption, reflection and transmission coefficients of the in-duct orifice are calculated by transfer function method. It is found that the sound coefficients are strongly dependent on the orifice opening size and frequency.

In the presence of a mean flow in the duct, vortex shedding and pressure fluctuation distribution become quite different from those calculated for the case without a mean flow. The vortices only shed in the direction of the flow. The sound absorption coefficient Δ_A is calculated and compared with that obtained for the case without a mean flow. Again, the calculated Δ_A is highest for the smallest D/H and lowest for the largest D/H. The results further show that the distribution of Δ_A with fH/c for both cases (with and without mean flow) is fairly similar, especially the overall level of Δ_A over the range of fH/c investigated. This shows that the mean flow essentially has no effect on the level of Δ_A over the range of D/H examined.

Acknowledgments

Support from the Research Grants Council of the HKSAR Government under Projects PolyU 5174/02E and PolyU 1/02C and the Internal Competitive Research Grant of The Hong Kong Polytechnic University under Project A–PF32 is gratefully acknowledged.

References

[1] U. Ingard, H. Ising, Acoustic nonlinearity of an orifice, *Journal of the Acoustical Society of America* 42 (1967) 6–17.
[2] A. Cummings, Acoustic nonlinearity and power losses at orifices, *AIAA Journal* 22 (1984) 786–792.
[3] F. Van Herpe, D.G. Crighton, P. Lafon, Noise Generation by Turbulent Flow in a Duct Obstructed by a Diaphragm, AIAA Paper 95-035, 1995.
[4] M. Salikuddin, K.K. Ahuja, Acoustic power dissipation on radiation through duct terminations: experiments, *Journal of Sound and Vibration* 91 (1983) 479–485.
[5] X.D. Jing, X.F. Sun, Sound-excited flow and acoustic nonlinearity at an orifice, *Physics of Fluids* 14 (2002) 268–276.
[6] A. Cummings, I.J. Chang, The transmission of intense transient and multiple frequency sound waves through an orifice plate with mean flow, *Revue de Physique Appliquee* 21 (1986) 151–161.
[7] J.C. Wendoloski, Sound absorption by an orifice plate in a flow duct, *Journal of the Acoustical Society of America* 104 (1998) 122–132.
[8] R.C.K. Leung, X.M. Li, R.M.C. So, Comparative study of nonreflecting boundary condition for one-step duct aeroacoustics simulation, *AIAA Journal* 44 (2006) 664–667.
[9] F.Q. Hu, A stable, perfectly matched layer for linearized Euler equations in unsplit physical variables, *Journal of Computational Physics* 173 (2001) 455–480.
[10] S.K. Lele, Compact finite difference schemes with spectral-like resolution, *Journal of Computational Physics* 103 (1992) 16–42.
[11] M.R. Visbal, D.V. Gaitonde, High-order-accurate methods for complex unsteady subsonic flows, *AIAA Journal* 37 (1999) 1231–1239.

[12] J.Y. Chung, D.A. Blaser, Transfer function method of measuring in-duct acoustic properties. I. Theory, *Journal of the Acoustical Society of America* 68 (1980) 907–913.
[13] J.Y. Chung, D.A. Blaser, Transfer function method of measuring in-duct acoustic properties. II. Experiment, *Journal of the Acoustical Society of America* 68 (1980) 914–921.
[14] F.J. Fahy, *Sound Intensity*, second ed., E & FN SPON, London, 1995.
[15] K.R. Holland, P.O.A.L. Davies, The measurement of sound power flux in flow ducts, *Journal of Sound and Vibration* 230 (2000) 915–932.
[16] I.D.J. Dupère, A.P. Dowling, Absorption of sound near abrupt area expansions, *AIAA Journal* 38 (2000) 193–202.
[17] B.F. Armaly, F. Durst, J.C.F. Pereira, B. Schönung, Experimental and theoretical investigation of backward-facing step flow, *Journal of Fluid Mechanics* 127 (1983) 473–496.